

Impact of visual perception on the performance of Color Shift Keying modulation in IEEE 802.15.7

Pankil M. Butala^{1,2}, Hany Elgala^{1,3} and Thomas D.C. Little^{1,4}

¹*Multimedia Communication Laboratory and Smart Lighting Engineering Research Center
Boston University, Boston, MA 02215, USA
{²pbutala,³helgala,⁴tdcl}@bu.edu*

Abstract: The IEEE 802.15.7 standard defines specifications for short-range optical wireless communication (OWC) using visible light. The standard specifies color shift keying (CSK) as the preferred modulation scheme for indoor OWC while simultaneously providing illumination. This article considers the performance of M -ary CSK under the linear system model as specified in the standard. In light of illumination requirements, human eye's optical perception introduces unique non-linearities in the CSK signaling chain. It is shown that these non-linearities introduce performance penalties of more than 15 dB, 10 dB, and 5 dB for $M = 4, 8$, and 16-CSK respectively. A new metric called luminous-signal-to-noise ratio (LSNR) is also introduced to fairly compare performance of any two OWC signaling schemes operating at a user defined illumination intensity level and is used to compare performance of M -ary CSK implemented with different colored sources. At a target bit error rate of $\leq 10^{-3}$, simulation results indicate that clipping negative receiver output does not have an impact on M -ary CSK performance.

© 2015 Optical Society of America

OCIS codes: (060.2605) Free-space optical communication, (060.4080) Modulation, (060.4510) Optical communications

References and links

1. “Cisco visual networking index: forecast and methodology, 2013-2018,” (2014).
2. H. Elgala, R. Mesleh and H. Haas, “Indoor optical wireless communication: potential and state-of-the-art,” IEEE Comm Mag. **49**(9), 56–62 (2011).
3. J. Gancarz, H. Elgala and T.D.C. Little, “Impact of lighting requirements on VLC systems,” IEEE Comm Mag. **51**(12), 34–41 (2013).
4. M. Rahaim and T.D.C. Little, “Towards Practical Integration of Dual-Use VLC within 5G Networks,” to appear in IEEE Wireless Comm. (2015).
5. J. Armstrong “OFDM for Optical Communications,” J. Lightwave Tech. **27**(3), 189-204 (2009).
6. P. Butala, H. Elgala and T.D.C. Little, “Sample indexed spatial orthogonal frequency division multiplexing,” Chin. Opt. Lett. **12**(9), 090602 (2014)
7. A. Yokoi, J. Son and T. Bae, “CSK constellation in all color band combinations,” <https://mentor.ieee.org/802.15/dcn/11/15-11-0247-00-0007-csk-constellation-in-all-color-band-combinations.pdf> (2011).
8. P. Butala, J. Chau and T.D.C. Little, “Metameric modulation for diffuse visible light communications with constant ambient lighting,” Intl. Workshop on Opt. Wireless Comm. (IWOW), 1-3 (2012).
9. “IEEE Standard for Local and Metropolitan Area Networks—Part 15.7: Short-Range Wireless Optical Communication Using Visible Light,” (2011).
10. S. Rajagopal, R.D. Roberts and S-K Lim, “IEEE 802.15.7 visible light communication: modulation schemes and dimming support,” IEEE Comm. Mag. **50**(3), 72-82 (2012).

-
11. R. Singh, T. O'Farrell and J.P.R. David, "Performance evaluation of IEEE 802.15.7 CSK physical layer," Globecom Workshops, IEEE 1064-1069 (2013).
-

1. Introduction

The proliferation of mobile devices including smartphones, tablets, and laptop computers is driving the need for increased capacity in wireless networks. Current forecasts [1] show that our wireless infrastructure must continually improve to sustain this level of growth. However, there remains an imbalance between the devices' ability to consume data and the networks' ability to service their demand. Traffic "offloading" has become the mitigation strategy whereby wireless access technologies such as WiFi are exploited for their localized capacity and links to wired infrastructure. However, these radio frequency (RF) solutions share limited available spectrum and face both scale and deployment challenges. Light-based media, in contrast, offer new spectrum opportunities and characteristics such as line-of-sight and security. This is fueling recent research on how to achieve light-based communication [2]. At the same time, advances in solid state materials have yielded highly-efficient light emitting diodes (LED) that have upended the lighting industry. Lighting companies now compete to replace all existing lighting with the new energy-efficient LED devices. Because lighting is well positioned to support human activities, it is also well positioned to serve as a highly localized wireless access vehicle by modulating the visible spectrum (380 nm – 780 nm). This model is called the "dual use" of lighting and communication. In a practical implementation, overhead luminaires provide light and data downlink as an offload medium, being augmented by the availability of other media including RF as part of a heterogeneous network [3, 4].

Visible light communication (VLC) uses intensity-modulation direct-detection (IM/DD) for wireless data transfer. Different modulation schemes used in conjunction with IM/DD have been proposed for use with VLC. Optical orthogonal frequency division multiplexing (O-OFDM) schemes provide high spectral efficiency for a single-input single-output (SISO) VLC channel [5]. To achieve better spectral efficiency, multiple-input multiple-output (MIMO) techniques exploiting dimensions of space and color have also been documented [6–8].

The IEEE standard for short-range optical wireless communication (OWC) using visible light specifies color shift keying (CSK) as the modulation technique of choice under the physical layer (PHY) III specifications [9]. For the rest of this article, the noun 'standard' shall imply the IEEE 802.15.7 standard, specifically chapter 12 on PHY III specifications as in reference [9]. The standard outlines linear system configurations with M -ary CSK to achieve up to 96 Mb/s data rate. Reference [10] provides an overview of modulation and dimming techniques specified within the standard while reference [11] studies select color bands for CSK.

This article studies M -ary CSK for all color band combinations as outlined in the standard and then extends the study to include practical implementation constraints: (a) non-linearity in visual perception introduces non-linearity in illumination to radiant flux transformations and vice versa and (b) user defined target illumination intensity level. In the process, a new metric – luminous-signal-to-noise ratio (LSNR) is introduced to compare performance of different signaling schemes at a target illumination intensity level.

An overview of CSK modulation technique is provided in Section 2. The linear CSK model as described in the standard is then outlined in Section 3. CSK performance considerations in a practical scenario due presence of non-linearity introduced by color to radiant flux transformation is considered in Section 4. Section 5 introduces LSNR and CSK performance considerations due to practical illumination constraints. Section 6 concludes the article.

2. Color Shift Keying

LED based luminaires are energy efficient and are thus being widely adopted in indoor spaces to provide illumination. In order to dynamically control the rendered illumination spectrum, luminaires contain multiple elements of at least three colors of LEDs. Different rendered spectra, or spectral power distributions (SPDs), can be generated by mixing different ratios of radiant flux emitted from the multiple LEDs comprising a luminaire. Each resulting SPD realizes a different color mix to the human eye.

Any SPD within the visible range of electromagnetic spectrum can produce a stimulus when incident on the sensors of the human eye (rod and cones) and has a color associated with it. This color can also be represented by its intensity, hue and saturation. While intensity is a measure of the total power comprising the SPD, hue and saturation are subjective parameters analogous to mean and spread of the wavelengths comprising the SPD and are quantified by a chromaticity coordinate. The *commission internationale de l'eclairage* (CIE) has specified the CIE 1931 XYZ color space (CIE-CS) that provides a mathematical model to represent the chromaticity of radiation in the visible range as a point in a 2-dimensional plane. Let a luminaire be comprised of three types of LEDs, namely LED_n ; $n \in \{i, j, k\}$. The chromaticity of each LED can be represented by a coordinate (x_n, y_n) on the CIE-CS. When different intensities of radiant flux emitted by three types of LEDs are combined, the chromaticity coordinate of the resultant SPD will lie inside the triangle formed by coordinates of the LEDs themselves.

CSK is a modulation technique in which information is transmitted through changes in chromaticity coordinates. This can be achieved by varying the intensities of LED_n over time. To select sources for CSK implementation, the standard specifies 7 different color bands - CB_u ; $0 \leq u < 7$ by splicing the visible spectrum range into 7 contiguous segments as shown in Table 1. The center wavelength of each segment as represented on CIE-CS is illustrated in Fig. 1. Note that even though center wavelengths of CB_4 , CB_5 and CB_6 are 47 nm – 50 nm apart, the distance between their chromaticity coordinates is very small. The CIE-CS is designed such that the SPD resulting from identical flux emitted by the three primary sources maps to coordinate $(1/3, 1/3)$ which is shown in Fig. 1. We can define a color sector on the CIE-CS as the region enclosed by a color band on the perimeter and coordinate $(1/3, 1/3)$. Though not explicitly mentioned in the standard, it is assumed that SPD of each LED_n must belong to a different color sector. To study the performance of CSK independent of specific LED characteristics, it is generally assumed that the chromaticity coordinate of an LED belonging to a color sector corresponds to the center wavelength of a color band CB_u at the perimeter of the sector as illustrated in Fig. 1.

CB_u	Band (nm)	Center (nm)	x	y
CB ₀	380 - 478	429	0.169	0.007
CB ₁	478 - 540	509	0.011	0.733
CB ₂	540 - 588	564	0.402	0.597
CB ₃	588 - 633	611	0.669	0.331
CB ₄	633 - 679	656	0.729	0.271
CB ₅	679 - 726	703	0.734	0.265
CB ₆	726 - 780	753	0.734	0.265

Table 1: Color bands.

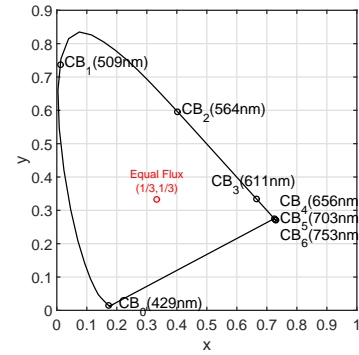


Fig. 1: Color band centers on CIE-CS.

To implement CSK using 3 types of LEDs, the standard defines different sets of 3 color bands and calls each set a color band combination (CBC). The 3 different types of LEDs forming a CBC are ordered in a descending manner based on the center wavelength of the color band they belong to and each such band is called ‘band i’, ‘band j’ and ‘band k’ respectively. 9 such CBC_v ; $1 \leq v \leq 9$ are defined in the standard and are outlined in Table 2. For the rest of this article, generalized notation CB_n^v will be used to indicate color band of type $n \in \{i, j, k\}$ belonging to CBC_v . Thus in Table 2, the cell representing row for CBC_v and column for band n provides index u for the color band represented by notation CB_n^v . Using this notation $\text{CB}_i^1 \equiv \text{CB}_6$ while $\text{CB}_j^2 \equiv \text{CB}_1$ and so on.

For an M -ary CSK using CBC_v , the design rules to compute the M different constellation points are provided in the standard and their values are outlined in [7]. Let $\text{C}_n^v \equiv (x_n^v, y_n^v)$ be chromaticity coordinate corresponding to CB_n^v . Let $\text{C}_m \equiv (x_m, y_m)$; $0 \leq m < M$ be chromaticity coordinate corresponding to m^{th} codeword. Then Table 3 outlines the design rules for computing the constellation points. C_n^v can be looked up from Table 2 and Table 1. Using these values, remaining C_m can then be computed using rules from Table 3. Normalized constellation design rules for M -ary CSK are illustrated in Fig. 2. Points I, J and K represent normalized coordinates for the n color bands comprising a CBC.

CSK is implemented in conjunction with IM/DD over the optical channel. This channel can be modeled as a linear time invariant system with additive white Gaussian noise (AWGN) and mathematically represented as in Eq.(1)

$$\mathbf{Y} = \mathbf{H}\mathbf{X} + \mathbf{W} \quad (1)$$

where \mathbf{X} is an n_{tx} dimensional vector containing transmit optical powers for each band n , \mathbf{H} is a $n_{rx} \times n_{tx}$ dimensional channel matrix, \mathbf{W} is a n_{rx} dimensional noise vector and \mathbf{Y} is an n_{rx} dimensional receive vector. Channel matrix \mathbf{H} includes the responsivities of the receive elements.

In M -ary CSK, $n_{tx} = 3$ types of LEDs are used to generate M different SPDs corresponding to M different chromaticity coordinates. Each chromaticity coordinate represents a codeword that encodes $\log_2(M)$ bits. In order to transmit information, the luminaire irradiates an SPD corresponding to the desired transmit codeword. The clock rate at the luminaire is of the order of tens of MHz. This rate is much higher than which can be perceived by human eye as flicker. In addition, the CSK signaling chain can include a scrambler that ensures data and thus codewords are pseudo-randomly distributed thus mitigating color flicker.

At the receiving elements, each SPD produces a different electrical response signal. The

Color band combination CBC_v	Color band ‘ u ’ for CBC_v		
	Band i	Band j	Band k
CBC_1	6	2	0
CBC_2	6	1	0
CBC_3	5	2	0
CBC_4	5	1	0
CBC_5	4	2	0
CBC_6	4	1	0
CBC_7	3	2	0
CBC_8	3	1	0
CBC_9	2	1	0

Table 2: Color bands combinations as specified by the standard.

m	M = 4	M = 8	M = 16
0	C_j^v	$(2C_4+C_5)/3$	C_j^v
1	$(C_i^v+C_j^v+C_k^v)/3$	$(2C_a+C_b)/3; C_a=(C_b+C_3+C_5)/3; C_b=(C_4+C_5)/2$	$(C_0+C_3+C_5)/3$
2	C_k^v	$(2C_a+C_b)/3; C_a=(C_b+C_3+C_7)/3; C_b=(C_4+C_7)/2$	$(C_3+C_6+C_{10})/3$
3	C_i^v	$(C_5+C_7)/2$	$(2C_0+C_9)/3$
4		C_j^v	$(C_0+2C_8)/3$
5		C_k^v	$(2C_0+C_8)/3$
6		$(2C_4+C_7)/3$	$(C_0+C_8+C_9)/3$
7		C_i^v	$(C_4+C_5+C_6)/3$
8			C_i^v
9			C_k^v
10			$(C_0+2C_9)/3$
11			$(C_9+C_{10}+C_{15})/3$
12			$(2C_8+C_9)/3$
13			$(C_4+C_8+C_{12})/3$
14			$(C_6+C_{12}+C_{15})/3$
15			$(C_8+2C_9)/3$

Table 3: Design rules to compute constellation points for M -ary CSK. Each row computes C_m , the chromaticity coordinate for m^{th} codeword for any given CBC_v. C_n^v is the chromaticity coordinate of color band $n \in \{i, j, k\}$ belonging to CBC_v.

signal output from each receiving element is corrupted by shot noise of variance σ_{sh}^2 due to ambient light and thermal noise of variance σ_{th}^2 due to trans-impedance amplifier as shown in Eq.(2)

$$\begin{aligned}\sigma_{sh}^2 &= 2q < i > B \\ \sigma_{th}^2 &= \frac{4k_B TB}{R_f}\end{aligned}\quad (2)$$

where $< i >$ is average current generated in the photodiode due incident ambient light, q is charge of an electron, k_B is Boltzmann's constant, T is the temperature in Kelvin and R_f is the amplifier feedback resistance and B is the channel bandwidth. The signal-to-noise ratio (SNR) can then be defined as in Eq.(3)

$$\text{SNR} \triangleq \frac{\text{Tr}\{\mathbf{H}\mathbf{X}\mathbf{X}^*\mathbf{H}^*\}}{\sigma_{nt}^2} \quad (3)$$

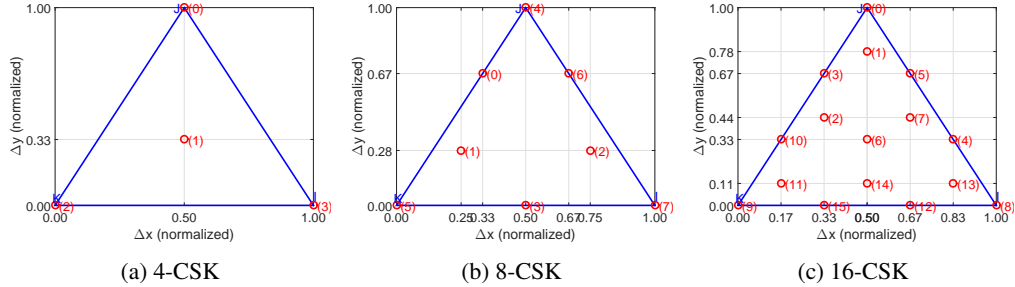


Fig. 2: M -ary CSK (normalized) constellation design rules.

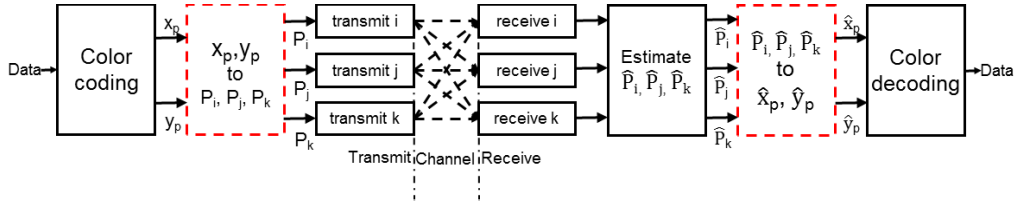


Fig. 3: Block diagram of CSK signal chain. Implementation of red dashed blocks differentiates the linear and the non-linear system models.

where $\text{Tr}\{\cdot\}$ is the matrix trace operator, $*$ indicates transpose and $\sigma_{nt}^2 = \sigma_{sh}^2 + \sigma_{th}^2$ is the total noise variance. SNR in decibel is then computed as $10\log_{10}(\text{SNR})$.

Having received vector \mathbf{Y} , least squares estimate of transmitted vector ($\hat{\mathbf{X}}$) can be made by Eq.(4).

$$\hat{\mathbf{X}} = (\mathbf{H}^* \mathbf{H})^{-1} \mathbf{H}^* \mathbf{Y} \quad (4)$$

After estimating vector $\hat{\mathbf{X}}$, an estimate of transmitted chromaticity coordinates can be made and transmitted information can then be decoded. The process of transforming chromaticity coordinates to optical power and vice-versa gives rise to two different system models as described in further sections.

3. CSK: Linear system model

The linear CSK model treats the CIE-CS as a linear space to analyze CSK performance. This implies the inherent assumption that when irradiance from multiple transmitting elements is combined, the chromaticity coordinates of the resulting SPD is a linear combination of the chromaticity coordinates of the SPDs of individual transmitting elements. If $P_n; n \in \{i, j, k\}$ is the normalized radiant flux at the transmit or receive device associated with band n , Eq.(5) below taken from the standard provides the implied mathematical relationships between chromaticity coordinates of all bands and that of resultant SPD.

$$\begin{aligned} x_p &= P_i x_i + P_j x_j + P_k x_k \\ y_p &= P_i y_i + P_j y_j + P_k y_k \\ 1 &= P_i + P_j + P_k \end{aligned} \quad (5)$$

A block diagram of the CSK signaling chain is shown in Fig. 3. At the transmitting element, the data bit-stream is encoded to chromaticity coordinates (x_p, y_p) as computed from Table 3. Using Eq.(5), normalized P_n values are computed which are then scaled to achieve a given illumination target and thus transmit irradiance. A vector of scaled P_n values then forms the transmit vector \mathbf{X} . Without loss of generality, unity electrical to optical conversion at transmitter and unity responsivity (optical to electrical conversion) at the receiver is assumed. Receiving element for band n senses the incident flux and generates an electrical signal proportional to it. AWGN as computed from Eq.(2) is then added to each band n in the form of vector \mathbf{W} . The receiver output in presence of noise is represented by \mathbf{Y} . With the knowledge of the channel state and the receiver output, a least squares estimate of transmit vector $\hat{\mathbf{X}}$ is made using Eq.(4). Each element of $\hat{\mathbf{X}}$ then provides the estimates of transmitted flux represented by \hat{P}_n . Using these values, (\hat{x}_p, \hat{y}_p) are estimated using Eq.(5). Nearest neighbor decoder then estimates the transmitted coordinate and recovers the transmitted information. Thus for the linear system

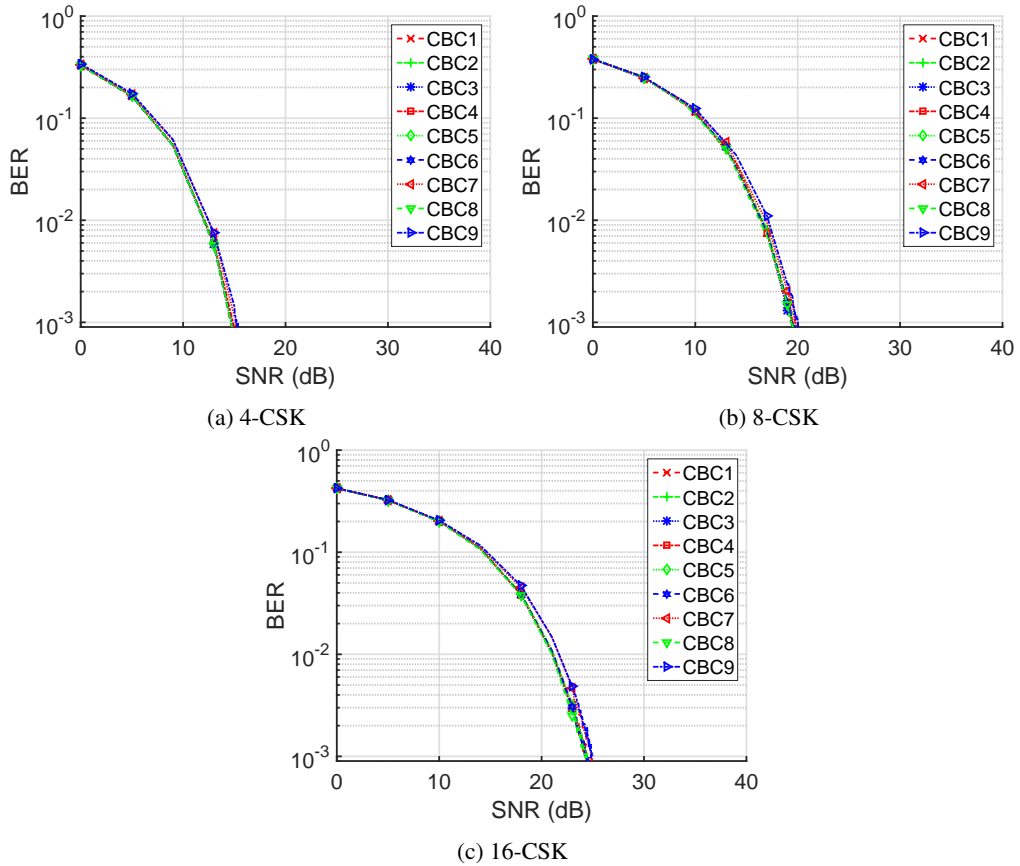


Fig. 4: BER vs SNR for linear model

model, Eq.(5) represents the $(x_p, y_p) \rightarrow P_n$ and $\hat{P}_n \rightarrow (\hat{x}_p, \hat{y}_p)$ transformations for the red dashed blocks of Fig. 3.

Monte-carlo simulations are performed to compute performance of M -ary CSK under the linear model for all CBC_v and Fig. 4 shows the results. CBC_2 performs the best whereas CBC_9 performs the worst, but only by a margin of about 0.6 dB. This performance is as expected. As seen from Table 2, CBC_2 is composed of CB_6 , CB_1 and CB_0 while CBC_9 is composed of CB_2 , CB_1 and CB_0 . Thus from values in Table 1 and Fig. 1, it can be seen that constellation points for CBC_2 are the most spread out and have the largest minimum distance between constellation points whereas for CBC_9 have the shortest spread and have the smallest minimum distance between constellation points. SNR of at least 15 dB, 20 dB and 25 dB are needed to achieve a target minimum bit error rate (BER) of 10^{-3} under the linear model for $M = 4$, 8 and 16 CSK respectively.

Fig. 5 shows received symbols for CBC_2 under the linear model. As expected, noise is spread normally along x and y dimensions forming a circular envelop around all constellation points. For $M = 8$ and $M = 16$, empty non-interfering regions devoid of received symbols can be seen in the figures. This indicates that these constellations could be better packed by defining additional points in the non-interfering regions. The constellations can then be further optimized to achieve better spectral efficiency. Note that in Fig. 5 (a), (b) and (c), some of the received symbols are located outside the color gamut (triangle IJK as outlined in Fig. 2) formed by the sources for

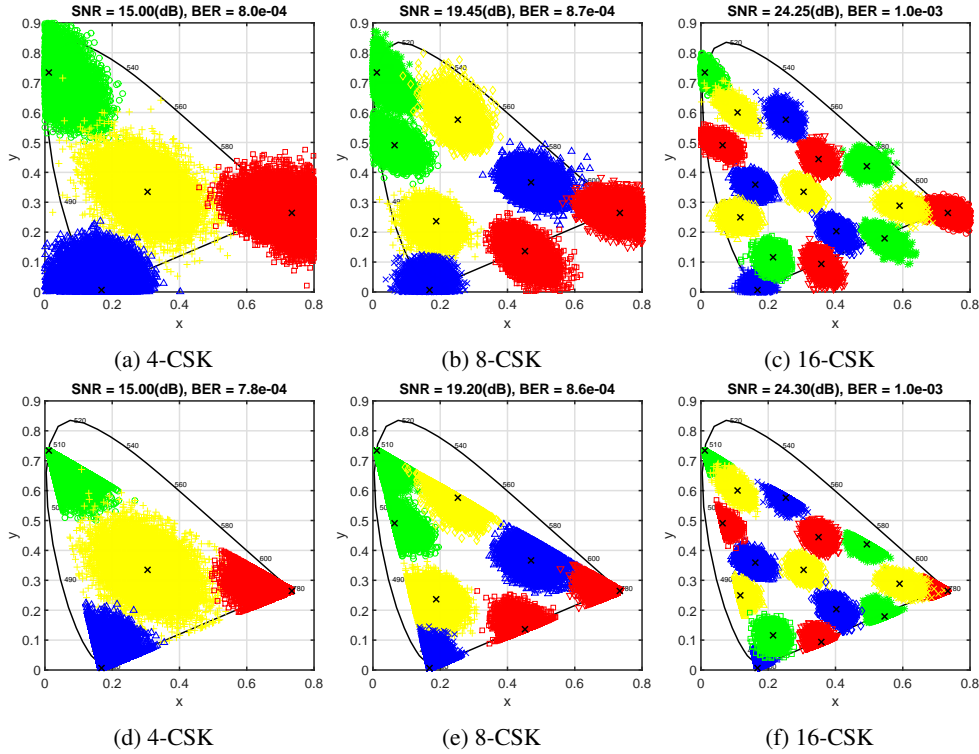


Fig. 5: Received symbols for CBC₂. (a),(b),(c): Receiver output not clipped. (d),(e),(f): Negative values of receiver output clipped at zero.

i, j and k bands. This would appear to violate the relationships on the CIE-CS model between coordinates of SPDs of individual sources and that of the resultant SPD formed by mixing the fluxes in different ratios. However, at the receiver, the received signals are influenced by noise (bipolar, zero-mean Gaussian) resulting in bipolar received values. Received signals with negative values when mapped back to the CIE-CS, can cause received ‘noisy’ symbols to lie outside of the gamut.

Since the transmitted radiant fluxes are always non-negative, it is possible to clip the receiver output prior to estimating the transmitted radiant flux. When negative receiver output is clipped at zero, estimated symbols are illustrated in Fig. 5 (d), (e) and (f). This clipping shows that the mapping back to CIE-CS is sensible. It can also be seen that at target BER of 10^{-3} , the clipping does not introduce any significant change in performance when compared to that without clipping.

While this linear system model is instructive to study M -ary CSK modulation and carry out a first order performance analysis, a practical CSK system incorporating human eye’s visual perception, is non-linear due to non-linearity of the CIE-CS. The $(x_p, y_p) \rightarrow P_n$ block at the transmitter and its counterpart and $\hat{P}_n \rightarrow (\hat{x}_p, \hat{y}_p)$ at the receiver (red colored dashed blocks in Fig. 3) introduce this non-linearity which significantly alters the M -ary CSK performance for a practical implementation. The effects of these practical constraints on a CSK system are studied in next few sections.

4. CSK: Non-linear system model

To understand the source of non-linearity in the CSK system, let's take a look at the CIE-CS which empirically models the human eye's visual perception of color for a stimulating SPD. Let $S_n(\lambda)$ be the SPDs of the transmit LEDs and P_n be the radiant flux associated with band n . Thus the aggregate transmitted SPD is given by Eq.(6).

$$W(\lambda) = \sum_{n \in \{i, j, k\}} P_n S_n(\lambda) \quad (6)$$

CIE-CS specification outlines three color matching functions - $x_c(\lambda)$, $y_c(\lambda)$ and $z_c(\lambda)$ as illustrated in Fig. 6. The tristimulus values for the three primary sources as defined in the CIE-CS are given by Eq.(7) and the chromaticity coordinates (x_p, y_p) of the resultant SPD $W(\lambda)$ are given by Eq.(8). From Eqs.(6-8) it can also be inferred that the relationship between P_n and (x_p, y_p) is non-linear.

$$\begin{aligned} X_W &= \int_{\lambda = 380 \text{ nm}}^{\lambda = 780 \text{ nm}} W(\lambda) x_c(\lambda) d\lambda \\ Y_W &= \int_{\lambda = 380 \text{ nm}}^{\lambda = 780 \text{ nm}} W(\lambda) y_c(\lambda) d\lambda \\ Z_W &= \int_{\lambda = 380 \text{ nm}}^{\lambda = 780 \text{ nm}} W(\lambda) z_c(\lambda) d\lambda \end{aligned} \quad (7)$$

$$x_p = \frac{X_W}{X_W + Y_W + Z_W}; y_p = \frac{Y_W}{X_W + Y_W + Z_W} \quad (8)$$

As outlined in prior sections, M -ary CSK modulation transmits information by varying the chromaticity coordinates of transmit SPD. In a practical implementation, a table of unique transformation ratios $P_i:P_j:P_k \rightarrow (x_p, y_p)$ can be pre-computed for each of the M constellation points. Referring back to Fig. 3, at the transmitter the data is color coded to obtain (x_p, y_p) coordinate to transmit. Given this coordinate, corresponding flux ratios $P_i:P_j:P_k$ can be looked up from the pre-computed table. The target illumination requirements provide the total radiant

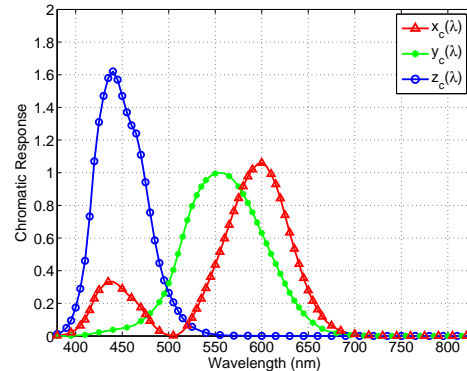


Fig. 6: CIE 1931 XYZ color matching functions.

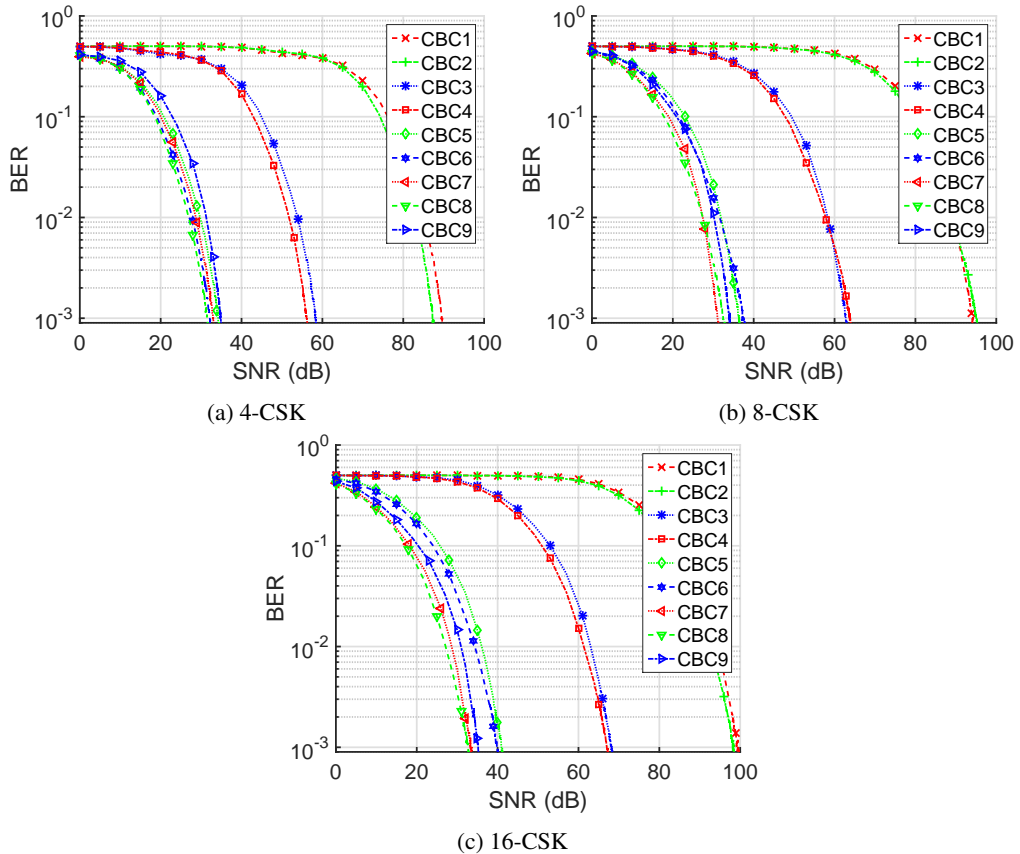


Fig. 7: BER vs SNR for all CBC

flux to output from the transmitting sources. With the flux ratio and the total radiant flux information, individual P_n for each band n can now be computed from Eq.(6). This transformation now forms the $(x_p, y_p) \rightarrow P_n$ block in the transmitter signaling chain. These transmitted flux are sensed by the receivers in presence of AWGN. The receivers generate an electrical output which is then used to compute an estimate of transmitted radiant fluxes \hat{P}_n . Eqs.(6-8), which now constitute the $\hat{P}_n \rightarrow (\hat{x}_p, \hat{y}_p)$ block in the receive signal chain, can then be used to estimate the transmitted coordinate (\hat{x}_p, \hat{y}_p) . Thus, the AWGN added to the received signal undergoes a non-linear transformation during $\hat{P}_n \rightarrow (\hat{x}_p, \hat{y}_p)$ process which skews the noise in the chromaticity plane of the CIE-CS. This causes additional performance penalties in a practical CSK system.

Fig. 7 shows performance of all the CBCs under this non-linear model. These curves are obtained by monte-carlo simulations similar to those performed for the linear model after substituting the $P_n \rightarrow (x_p, y_p)$ and $\hat{P}_n \rightarrow (\hat{x}_p, \hat{y}_p)$ blocks with the non-linear system model transformations. It can be observed that CBC₇ and CBC₈ perform relatively similar and are the best while CBC₁ performs the worst. Additionally, it is observed that CBC₁-CBC₄ perform significantly worse as compared to the rest. For CBC₁-CBC₄, the amount of radiant flux emitted by band i is 3-4 orders of magnitude greater than band j and 1-2 orders of magnitude greater than band k. Thus the $\hat{P}_n \rightarrow (\hat{x}_p, \hat{y}_p)$ conversion at the receiver is extremely sensitive to noise along the j and k bands as compared to that along the i band. This introduces significant errors in

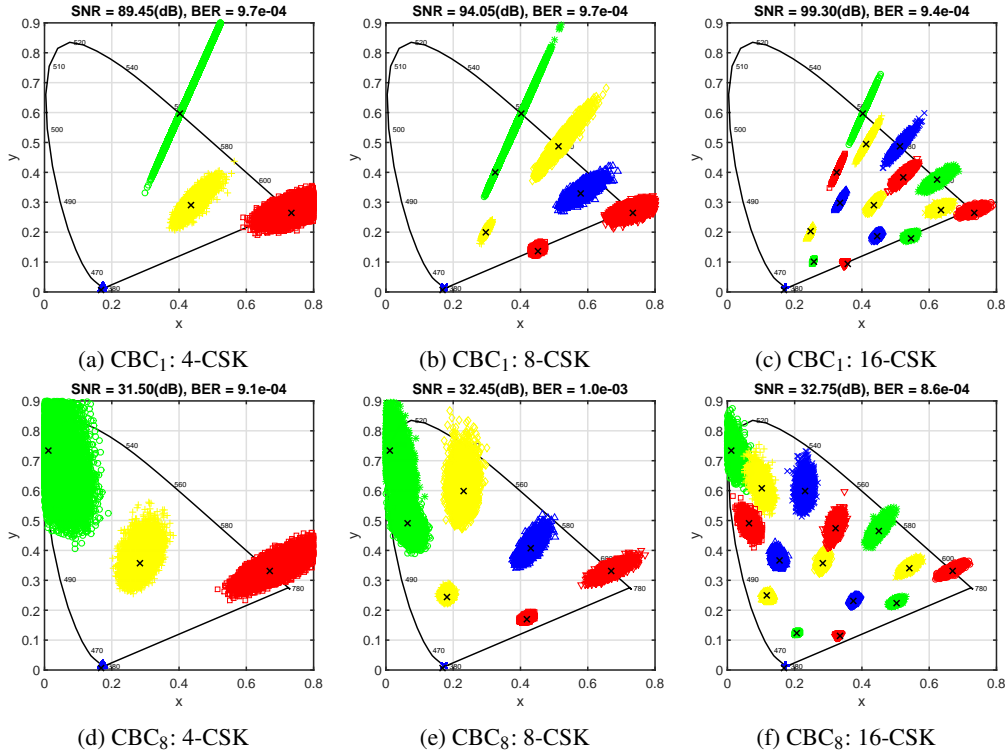


Fig. 8: Received symbols for non-linear model when receiver output is not clipped. Some received symbols are located outside the color gamut. Note that noise when transformed to chromaticity plane is no longer AWGN.

decoding received symbols.

Fig. 8 and Fig. 9 show received symbols for CBC_1 and CBC_8 under the non-linear model. Noise skew about the estimated coordinates can be observed in both figures. This noise skew is more prominent for CBC_1 where the signal power distribution along all bands is imbalanced. In contrast for CBC_8 , signal power is more uniformly spread across all bands. For Fig. 8, the negative receiver output is not clipped at zero. As mentioned earlier, in presence of noise (zero mean and Gaussian), some receiver output values can be negative and thus such received symbols are located outside the color gamut when transformed to CIE-CS space. The effect of clipping negative receiver output at zero can be seen in Fig. 9 where all received symbols now are located inside the color gamut. It can be seen that performance of both receiver signal processing techniques is similar, as such no one outperforms the other. It can be seen that AWGN introduced on \hat{P}_n gets skewed radially towards band k due to non-linearity in $\hat{P}_n \rightarrow (\hat{x}_p, \hat{y}_p)$ transformation and is no longer AWGN along the CIE-CS chromaticity plane. This generates an interesting outcome in that for CBC_8 , about 30 dB of SNR is needed to achieve target 10^{-3} BER for all of $M = 4, 8$ and 16 CSK. This happens because with increase in order M , the additional constellation points as defined in the standard happen to occupy non-interfering regions of the chromaticity plane thus increasing spectral efficiency without incurring any SNR penalty up to a point. The non-linearity of the CIE-CS introduces performance penalties of at least 15 dB, 10 dB and 5 dB for $M = 4, 8$ and 16 CSK respectively over CBC_2 (best case) in linear system model.

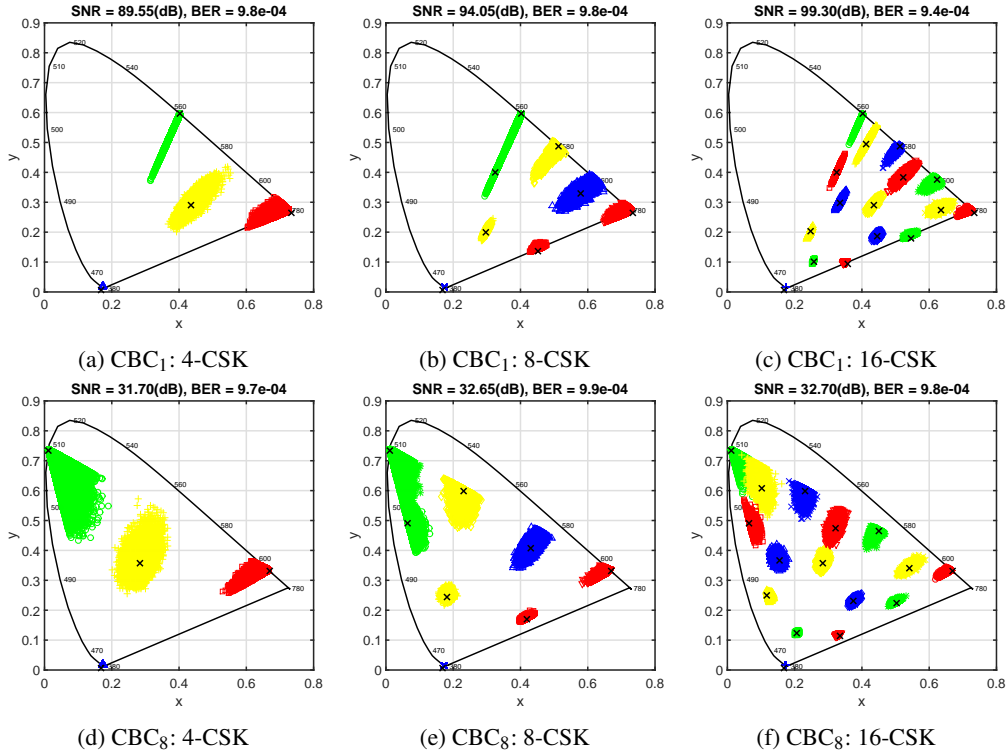


Fig. 9: Received symbols for non-linear model when negative values of receiver output are clipped at zero. All received symbols now are located inside the color gamut. Note that noise when transformed to chromaticity plane is no longer AWGN.

5. CSK: Performance under illumination constraints

5.1. Luminous-signal-to-noise ratio

In an indoor optical wireless system using lighting devices for wireless downlink access the luminaires need to simultaneously service illumination and optical wireless broadcast missions. Under this model, different colored PHY (example: different CBC_v) irradiate different amounts of radiant flux to achieve the same illumination intensity level. Thus, it is unfair to use SNR as a metric to compare performance of modulation schemes at same BER target using different colored PHY without first normalizing for illumination targets. Thus, in this section we introduce LSNR as a metric that takes into account the differences in radiant flux emitted by different PHY to achieve the same illumination intensity level. It should be noted that the LSNR metric is not specific to CSK, but instead can be used more generally to compare performance of any two optical modulation schemes that are operated at the same optical intensity levels.

Consider optical modulation scheme(s) which can be implemented with two different constellations C_a or C_b . The fluxes emitted by the two constellations are scaled to achieve a target illumination intensity level. Let both constellations on average emit I lumens of luminous flux. Let the luminous efficacy for the two constellations be specified by η_a and η_b in lumens-per-watt respectively. Then the corresponding average radiant flux emitted by the two constellations is given by $W_a = I/\eta_a$ and $W_b = I/\eta_b$ watts respectively. Let us define a luminous ratio $L_{ab} \triangleq (\eta_a/\eta_b) \equiv (W_b/W_a)$. Thus, for every 1 Watt of radiant flux emitted by C_a , C_b must emit L_{ab}

Watt of radiant flux to achieve the same illumination intensity level. Under the model where the luminaires service illumination along with communication, it is fair to compare the performance of the two schemes at these relative radiant flux levels instead of at the absolute radiant flux levels. Thus we define the LSNR metric in Eq.(9) as a means to compare performance of C_b versus that of C_a at same illumination levels.

$$\text{LSNR}_{ab} \triangleq \frac{\text{L}_{ab}^2 \text{Tr}\{\mathbf{H}\mathbf{X}_b\mathbf{X}_b^*\mathbf{H}^*\}}{\sigma_n^2} \quad (9)$$

where \mathbf{X}_b is the average radiant flux emitted by C_b . Thus, after computing BER vs SNR for the scheme employing C_a , BER vs LSNR can be computed for scheme employing C_b to compare its performance relative to that employing C_a at the same illumination levels.

5.2. Performance under illumination constraints

Fig. 10 shows performance of the 9 CBCs under the non-linear model when normalized for illumination constraints. The efficacies of all CBC for different M are specified in the legends. These values are used to normalize the performance of M -ary CSK for all CBC using CBC with highest efficacy as the reference for LSNR calculation. CBC₇, CBC₉ and CBC₉ are used as reference CBCs for $M = 4, 8$ and 16 CSK respectively. The effect of this is to shift all

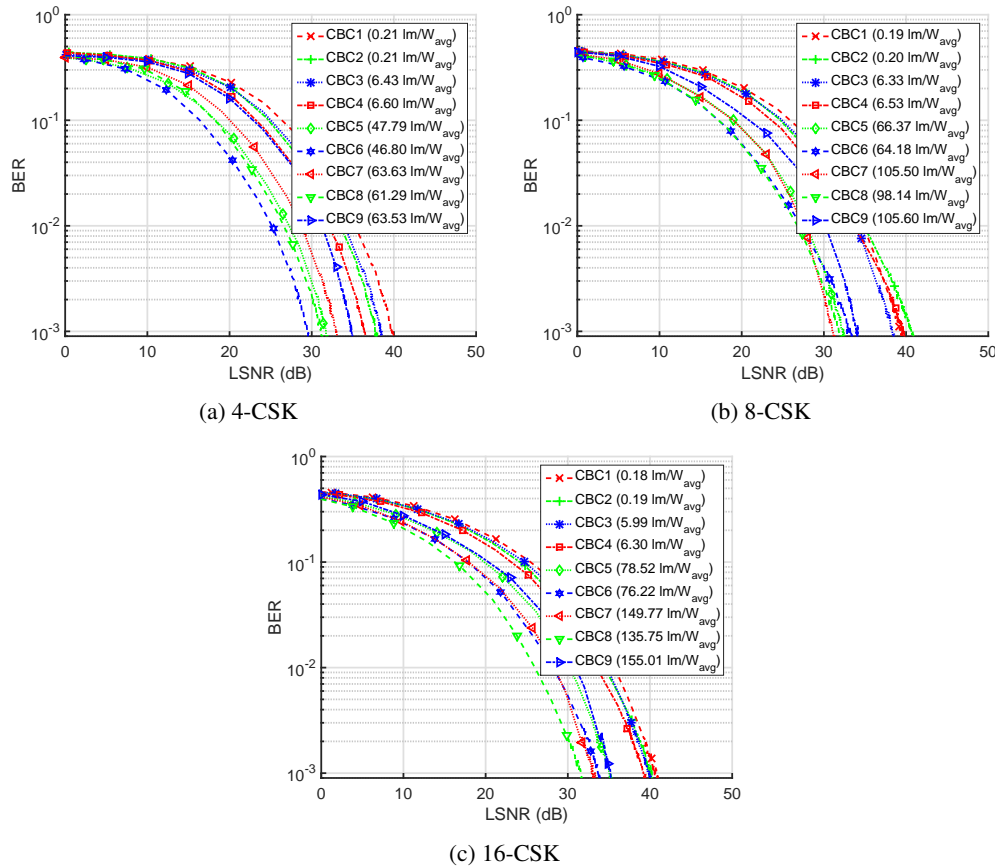


Fig. 10: BER vs LSNR for all CBC

curves (except the reference) from Fig. 7 towards left along the LSNR-axis depending on the L_{ab} values in Eq.(9). It can be observed that given a target illumination intensity level and for target 10^{-3} BER, CBC₆ performs the best for 4-CSK, CBC₇ and CBC₈ perform similar and better than others for 8-CSK and CBC₈ performs the best for 16-CSK. For CBC₁-CBC₄, due to their low luminous efficacy, one can use a much larger radiant flux to achieve target illumination levels and thus significantly improve their communication performance. However, this is achieved at the cost of poor energy efficiency. In contrast, CBC₇ and CBC₉ have relatively high luminous efficacy. This implies that these CBCs are restricted to emit a relatively lower radiant flux (and thus low signal powers) to achieve target illumination level thus affecting their communication performance. These results also highlight the necessary tradeoff between goals of energy efficient lighting and good communication performance; thus making a case for an optimization between the two divergent goals.

6. Conclusion

This article explores the performance of all CBCs as specified for M -ary CSK in the IEEE 802.15.7 standard. Under the linear system model CBC₂ performs the best and needs SNR of at least 15 dB, 20 dB and 25 dB to achieve target $\text{BER} = 10^{-3}$ for $M = 4, 8$ and 16-CSK respectively. The non-linear system model is then considered due to the unique non-linear visual perception characteristics of human eye. It is shown that the non-linearity of the CIE-CS implies that the AWGN introduced to the received signal is skewed and is no longer AWGN when transformed to the chromaticity plane. Under the non-linear system model, CBC₇ and CBC₈ perform relatively similar and are better than all other CBCs. A performance penalty of at least 15 dB, 10 dB and 5 dB incurred for the practical non-linear model as compared to CBC₂ in linear model for $M = 4, 8$ and 16-CSK respectively. A new LSNR metric is proposed to compare performance of any two schemes (and not just CSK) using the visible spectrum for wireless communication and lighting after normalizing signal powers to achieve a target illumination intensity level. Performance comparisons of M -ary CSK for all CBCs then reveal that CBC₆ performs the best for 4-CSK, CBC₇ and CBC₈ perform similar and better than others for 8-CSK and CBC₈ performs the best for 16-CSK.

For IM/DD signaling scheme, the receiver output is always expected to be non-negative in absence of noise. For some O-OFDM systems, clipping negative receiver output has been shown to improve performance by eliminating some noise. On the contrary, for M -ary CSK, the performance in presence or absence of clipping the negative receiver output does not seem to differ significantly. This does not imply that noise in the negative receiver output is orthogonal to signal itself. The negative receiver output pushes the received symbol outside the color gamut on the CIE-CS. In the presence of relatively high SNR, the received symbol is still located closer to the expected constellation point thus does not introduce any additional errors.

Optimal performance of CSK can be seen as a tradeoff between the illumination and communication missions. There is further scope to optimize the M -ary CSK constellations under the practical non-linear model by selecting optical sources centered at different wavelengths than those considered in the standard. After characterizing skew for AWGN along the chromaticity plane, constellation points can be optimally positioned and optimal receiver architectures can be introduced to further improve the M -ary CSK performance.

Acknowledgment

This work was supported by the Engineering Research Centers Program of the National Science Foundation under NSF Cooperative Agreement No. EEC-0812056.